ChemComm

COMMUNICATION

View Article Online
View Journal | View Issue

Cite this: *Chem. Commun.*, 2015, **51**, 14326

Received 16th July 2015,
Accepted 5th August 2015

DOI: 10.1039/c5cc05931c

www.rsc.org/chemcomm

Characterization of a heterobimetallic nonheme Fe(III)–O–Cr(III) species formed by O_2 activation†

Ang Zhou, Scott T. Kleespies, Katherine M. Van Heuvelen‡ and Lawrence Que Jr.*

We report the generation and spectroscopic characterization of a heterobimetallic $[(TMC)Fe^{III}–O–Cr^{III}(OTf)_4]$ species (1) by bubbling O_2 into a mixture of $Fe(TMC)(OTf)_2$ and $Cr(OTf)_2$ in $NCCH_3$. Complex 1 also formed quantitatively by adding $Cr(OTf)_2$ to $[Fe^{IV}(O)(TMC)(NCCH_3)]^{2+}$. The proposed O_2 activation mechanism involves the trapping of a $Cr–O_2$ adduct by $Fe(TMC)(OTf)_2$.

Oxygen activation is generally carried out by metalloenzymes with mononuclear or homodinuclear iron or copper active sites.[1–3] However there are two notable exceptions to this generalization, namely the heme/copper center of cytochrome oxidase essential for mammalian respiration[1,4,5] and the nonheme Fe–O–Mn center of Class 1c ribonucleotide reductases found in pathogenic bacteria.[6,7] There has been significant progress in obtaining synthetic models for the heme/copper center of cytochrome oxidase,[8–10] but less effort has been devoted to the synthesis of nonheme (μ-oxo)heterobimetallic complexes. In 1992 Wieghardt described a series of carboxylate-bridged $(TACN)Fe^{III}–O–M(Me_3TACN)$ ($M = Cr^{III}$ or Mn^{III}, TACN = 1,4,7-triazacyclononane, Me_3TACN = 1,4,7-trimethyl-1,4,7-triazacyclononane) complexes obtained by hydrolysis between $FeCl_3(TACN)$ and $MCl_3(Me_3TACN)$ precursors.[11] More recently, Fukuzumi and Nam reported the crystal structure of a novel $Fe^{III}–O–Sc^{III}$ complex, which was obtained from the reaction of $[Fe^{IV}(O)(TMC)(NCCH_3)]^{2+}$ (TMC = 1,4,8,11-tetramethylcyclam) with $Sc(OTf)_3$.[12] However, no synthetic nonheme Fe–O–M complex (where M is a non-iron metal) has thus far been generated by O_2 activation. Here we report the characterization of $[(TMC)Fe^{III}–O–Cr^{III}(OTf)_4]$ (**1**) formed by oxygenating a mixture of $Fe(TMC)(OTf)_2$ and $Cr(OTf)_2$ in CH_3CN at −40 °C or reacting $[Fe^{IV}(O)(TMC)(NCCH_3)]^{2+}$ with 1 eq. of $Cr(OTf)_2$.

Bubbling O_2 into a solution of 1 mM $Fe(TMC)(OTf)_2$ and 1 mM $Cr(OTf)_2$ in CH_3CN at −40 °C rapidly elicited a UV-vis spectrum with bands at 358, 398, 447 and 558 nm (Fig. 1), suggesting the formation of a new species designated as **1**. This spectral pattern was not observed in the absence of either $Fe(TMC)(OTf)_2$ or $Cr(OTf)_2$ from the reaction mixture; $Fe(TMC)(OTf)_2$ simply did not react with O_2, but the reaction of $Cr(OTf)_2$ with O_2 gave rise to features at 358 and 445 nm (Fig. 1), distinct from those of **1**. Species **1** had a half-life of 10 h at −40 °C and rapidly decayed upon warming to RT. Taken together, these observations implicate both Fe and Cr in the formation of **1**.

ESI-MS analysis of the solution of **1** at −40 °C revealed dominant peaks at *m*/*z* 461.2 (positive mode) and 514.8 (negative mode) (Fig. S1, ESI†), which were not observed in oxygenated solutions lacking either $Fe(TMC)(OTf)_2$ or $Cr(OTf)_2$. The ions observed have masses and isotope distribution patterns that correspond to $[Fe(TMC)(OTf)]^+$ and $[CrO(OTf)_3]^-$, respectively. Furthermore, the $[CrO(OTf)_3]^-$ peak was upshifted by 2 units when $^{18}O_2$ was used, showing the incorporation of an oxygen atom from O_2 (Fig. S2, ESI†). Based on these results, we tentatively assign **1** as a heterobimetallic $[(TMC)Fe^{III}–O–Cr^{III}(OTf)_4]$ complex, which undergoes homolysis of the Fe–O bond to give rise to the observed mass spectral features.

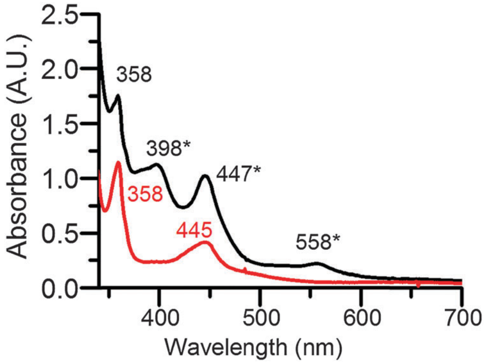

Fig. 1 UV-vis spectra observed in CH_3CN at −40 °C upon O_2 exposure of 1 mM $Cr(OTf)_2$ (red) and a mixture of 1 mM $Fe(TMC)(OTf)_2$ and 1 mM $Cr(OTf)_2$ (black). Bands with asterisks are associated with **1**.

Department of Chemistry and Center for Metals in Biocatalysis, University of Minnesota, 207 Pleasant St. SE, Minneapolis, Minnesota 55455, USA. E-mail: larryque@umn.edu

† Electronic supplementary information (ESI) available: Instrumental methods, synthetic procedures, and structural characterization. See DOI: 10.1039/c5cc05931c

‡ Current address: Department of Chemistry, Harvey Mudd College, Claremont, CA 91711, USA.

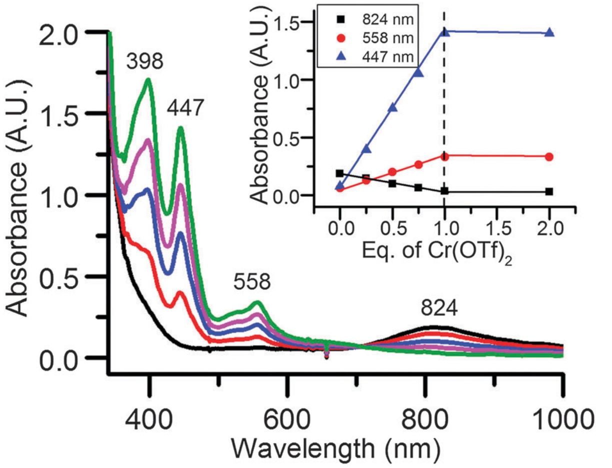

Fig. 2 UV-vis spectral titration of 0.45 mM $[Fe^{IV}(O)(TMC)(NCCH_3)]^{2+}$ in CH_3CN at −40 °C with $Cr(OTf)_2$. Black, 0 eq.; red, 0.25 eq.; blue: 0.5 eq.; magenta, 0.75 eq.; green, 1 eq. Inset: Titration plot. Inset: Formation of **1** *vs.* eq. $Cr(OTf)_2$ added into 0.45 mM $[Fe^{IV}(O)(TMC)(NCCH_3)]^{2+}$ in CH_3CN at −40 °C.

To test this hypothesis, we investigated the reaction of $[Fe^{IV}(O)(TMC)(NCCH_3)]^{2+}$[13] with $Cr(OTf)_2$ in CH_3CN at −40 °C as a more direct means of synthesizing putative species **1**. As shown in Fig. 2, the addition of $Cr(OTf)_2$ to $[Fe^{IV}(O)(TMC)(NCCH_3)]^{2+}$ in CH_3CN solution caused the instantaneous disappearance of its characteristic 824 nm peak concomitant with the growth of bands at 398, 447, and 558 nm that are assigned to **1**. Titration experiments (Fig. 2, inset) revealed that the transformation was complete upon addition of 1 eq. $Cr(OTf)_2$, strongly suggesting a 1 : 1 Fe : Cr stoichiometry for **1**. This solution also gave rise to ESI-MS spectra with the same dominant peaks as the complex generated by O_2 activation. A control experiment between $Cr(OTf)_2$ and PhIO did not elicit the same peaks as found in **1** (Fig. S3, ESI†), suggesting that $[Fe^{IV}(O)(TMC)(NCCH_3)]^{2+}$ acts more than just an oxygen atom donor to $Cr(OTf)_2$. These results demonstrate that **1** can be generated by either O_2 activation or inner-sphere electron transfer.

In order to obtain structural insight, Fe K-edge X-ray absorption spectroscopy studies were carried out on **1**. As shown in Fig. S4 (ESI†), the Fe K-edge of **1** was found at 7124.0 eV, which is comparable to those of known Fe^{III}(TMC) and related complexes.[14] Species **1** also exhibits a pre-edge feature that is associated with 1s-to-3d transitions with an area of 11 units. The Fourier-transformed EXAFS region revealed two prominent features at $R + \varDelta \sim 1.8$ Å and 3.2 Å (Fig. 3, left). The best fit of the data (fit #8 in Table S1, ESI†) consisted of 1 O/N scatterer at 1.81 Å, 5 O/N scatterers at 2.17 Å, 4 C scatterers at 2.91 Å and a Cr scatterer at a distance of 3.65 Å. The 2.17 Å and 2.92 Å scatterers arise from the supporting TMC ligand, while the 1.81 Å scatterer has an Fe–O distance typically found for oxo bridges in Fe^{III}–O–M^{III} complexes.[15] The 3.2 Å feature corresponds to a Cr scatterer at 3.65 Å; its intensity derives from multiple scattering pathways due to a linear Fe–O–Cr core. Indeed, the Fe···Cr distance is typical of the metal–metal distances found for linear Fe^{III}–O–M complexes[12,16,17] and exemplified by $[(py)(TPP)Cr^{III}–O–Fe^{III}(TMP)]$ (*r*(Fe···Cr) = 3.60 Å; py = pyridine; TPP = tetraphenylporphin dianion; TMP = tetramesitylporphin dianion).[18] We thus propose that **1** has the structure shown in Fig. 3 right.

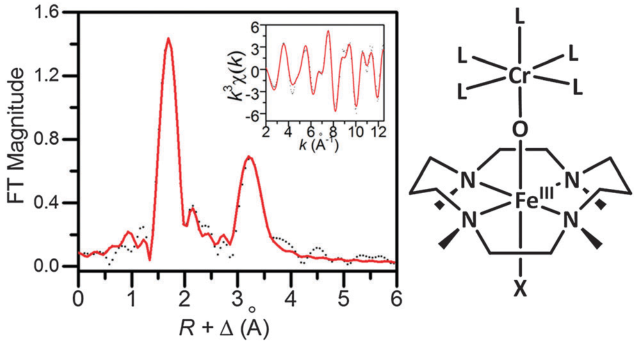

Fig. 3 Left: Fourier-transformed Fe K-edge EXAFS data for **1** (dotted black line) and corresponding best fit (solid red line, fit #8 in Table S1, ESI†). Inset shows unfiltered *k*-space data and its fit. Right: Proposed structure for **1** (L = CH_3CN or OTf; X = CH_3CN, NCO or NCS).

The proposed structure for **1** resembles that found in the crystal structures of the recently described $[(TMC)Fe^{III}–O–Sc^{III}(OTf)_4(L)]$ complex (**2**, L = H_2O or $NCCH_3$).[12] However, they differ in several respects. Although the Fe···M distances are essentially identical for **1** and **2**, the respective Fe–O and M–O distances are distinct. The Fe–O distance of 1.81 Å for **1** is 0.07 Å longer than that found for **2**, while the Cr–O distance of 1.84 Å (deduced from the difference between the Fe···Cr and the Fe–O distances from the EXAFS analysis, assuming ∠Fe–O–Cr ∼ 180°) is 0.07 Å shorter than the Sc–O distance of 1.91 Å observed for **2** in its crystal structures. The distinct M–O distances in **1** and **2** presumably reflect the difference between the more covalent Cr–O bond and the more ionic Sc–O bond, which also affect the corresponding Fe–O bond. Another feature distinguishing **1** from **2** is the intensity of the XAS pre-edge feature. Complex **1** exhibits a pre-edge area of 11 units, typical of a six-coordinate iron(III) center,[19,20] while **2** (L = $NCCH_3$) has a much larger pre-edge area of 32 units,[12] reflecting the square pyramidal geometry of its iron(III) center. Lastly, the four methyl groups of the TMC ligand are shown in Fig. 3 right as being oriented *anti* with respect to the oxo bridge, opposite to the orientation found crystallographically for the methyl groups in **2**.[12] Although we do not have direct proof, our main argument to favor the *anti* orientation over the *syn* one is the observed immediate formation of **1** upon $Cr(OTf)_2$ addition to a solution of $[Fe^{IV}(O)(TMC)(NCCH_3)]^{2+}$. As the TMC methyl groups are oriented *anti* to the oxo moiety in the precursor,[13] it seems unlikely that a change in their relative orientations could occur at −40 °C within this very short time scale.

The likelihood of a sixth ligand for the iron(III) center in **1** is supported by the change in the spectral features of **1** upon addition of NCS^- or NCO^-. As shown in Fig. 4, there are small shifts of the three bands, as well as increases in intensity. Titration experiments showed that only 1 eq. of NCS^- or NCO^- was needed to transform **1** fully into **1-NCS** or **1-NCO** (Fig. S5 and S6, ESI†). ESI-MS analysis of **1-NCS** and **1-NCO** revealed respective positive mode peaks at *m*/*z* 370 and 354, corresponding to $[Fe(TMC)(NCS)]^+$ and $[Fe(TMC)(NCO)]^+$ fragment ions (Fig. S7 and S8, ESI†), suggesting the occupation of the axial position *trans* to the

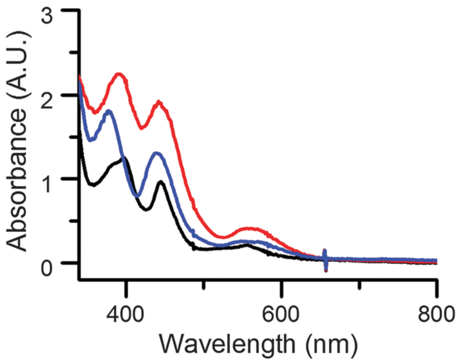

Fig. 4 UV-vis spectra of 0.3 mM **1** (black), **1-NCO** (blue), **1-NCS** (red) in CH_3CN at −40 °C. λ_{max} (ε_M) for **1**: 398 (3800), 447 (3000), and 558 (700). λ_{max} (ε_M) for **1-NCO**: 380 (6000), 438 (4200), and 560 (850). λ_{max} (ε_M) for **1-NCS**: 390 (7500), 442 (6300), and 560 (1400).

oxo bridge by these anions. Furthermore, **1-NCS** exhibits an Fe K-edge energy of 7124.3 eV, comparable to the 7124.0 eV value found for **1**. **1-NCS** also exhibits a pre-edge feature with an area of 9 units (Fig. S9, ESI†), which is close to the 11 units found for **1** but much smaller than the 32 units associated with **2**, showing that a six-coordinate iron(III) center in **1-NCS** is maintained. EXAFS analysis of **1-NCS** shows the presence of a linear Fe–O–Cr core like that in **1**, but with a 1.85 Å Fe–O bond and an Fe···Cr distance of 3.67 Å (Table S2 and Fig. S10, ESI†). The observed lengthening of the Fe–μ-O bond can be rationalized by the axial NCS^- binding to the iron(III) center. Based on all the information above, **1** is proposed to be a heterobimetallic μ-oxo species with an Fe–O–Cr core, and the Fe atom has a 6-coordinate environment with the axial position available for ligand substitution (Fig. 3, right).

Complex **1** was further studied by EPR and resonance Raman spectroscopy. It is EPR-silent, which is as expected due to antiferromagnetic coupling mediated by the oxo bridge between the Fe(III) and the Cr(III) centers, as seen for two other Fe(III)–O–Cr(III) complexes.[11,18] Excitation of **1** with a 568.2 nm laser elicits a resonance-enhanced vibration at 773 cm^{-1} (Fig. 5), which falls within the 700–900 cm^{-1} range found for the ν_{as}(Fe–O–Fe) modes of oxo-bridged diiron(III) complexes.[21] This assignment is corroborated by the observed downshift of this vibration to 730 cm^{-1} upon ^{18}O-substitution into the oxo bridge. Although a 35 cm^{-1} downshift for a diatomic Fe–O mode is predicted by Hooke's Law, the experimentally obtained ^{18}O shift is 43 cm^{-1}. This larger than predicted shift has also been reported for corresponding vibrations of several oxo-bridged diiron(III) complexes.[21] There is also a weaker feature found at 746 cm^{-1} that exhibits an upshift of 7 cm^{-1} upon ^{18}O-substitution; this is an unusual observation that we cannot explain. The 773 cm^{-1} vibration is also weakly enhanced upon 514.5 nm excitation but not observed with 457.9 or 647.1 nm irradiation, suggesting that the 558 nm absorption band can be associated with a transition of the Fe–O–Cr moiety.

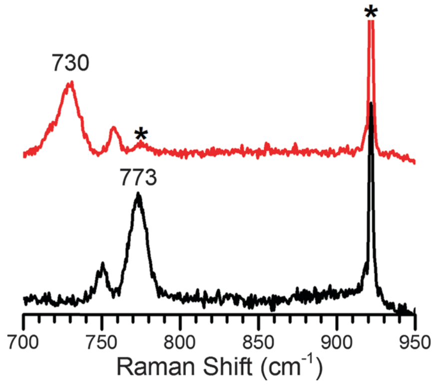

Fig. 5 Resonance Raman spectra of **1** in CH_3CN (λ_{ex} = 568.2 nm, 20 mW, 77 K). Black, ^{16}O; red, ^{18}O. Asterisks denote solvent peaks.

With the nature of **1** reasonably well characterized, we return to an analysis of the O_2 activation reaction results. Based on the molar extinction coefficients of **1** determined from the stoichiometric conversion of $[Fe^{IV}(O)(TMC)(NCCH_3)]^{2+}$ to **1** by $Cr(OTf)_2$, we conclude that **1** is produced in about 30% yield from the reaction of equimolar amounts of $Fe(TMC)(OTf)_2$ and $Cr(OTf)_2$ to O_2. The yield of **1** was unchanged by increasing the $Fe(TMC)(OTf)_2/Cr(OTf)_2$ ratio from 1 to 10 ($[Cr(OTf)_2]$ = 1 mM) (Fig. S11, ESI†), suggesting that $Cr(OTf)_2$ is the limiting reagent. In contrast, the yield of **1** increased to 95% when the concentration of $Fe(TMC)(OTf)_2$ was fixed at 1 mM and the $Cr(OTf)_2$ concentration was raised from 1 mM to 10 mM (Fig. S12, ESI†). Therefore, the % yield of **1** is dependent on the amount of $Cr(OTf)_2$, but not on the amount of $Fe(TMC)(OTf)_2$. These results can be rationalized by the O_2 activation pathway proposed in Scheme 1, in which the four electrons needed to reduce O_2 to the oxidation level of water are provided by 1 eq. $Fe(TMC)(OTf)_2$ and 3 eq. $Cr(OTf)_2$, not unlike the four redox-active centers required for O_2 activation by cytochrome oxidase.[4] In the present case, we postulate that O_2 initially binds to the O_2-sensitive $Cr(OTf)_2$ to form a transient adduct (analogous to that characterized by Nam in the reaction of $[Cr^{II}(TMC)Cl]^+$ with O_2[22]) that is then trapped by $Fe(TMC)(OTf)_2$ to generate a yet unobserved Fe^{III}–O–O–Cr^{III} peroxo-bridged intermediate. This intermediate is then reduced by another 2 eq. $Cr(OTf)_2$ to form **1**. Thus the *ca.* 30% yield of **1** observed under limiting Cr conditions reflects the 1 : 3 stoichiometry of $Fe(TMC)(OTf)_2/Cr(OTf)_2$ needed to make **1**. On the other hand, under limiting Fe conditions, enough Cr–O_2 adduct is formed to react with all the available $Fe(TMC)(OTf)_2$ to convert the latter almost quantitatively to **1**.

In conclusion, a heterobimetallic nonheme species **1** with an Fe–O–Cr core has been generated from both O_2 activation and

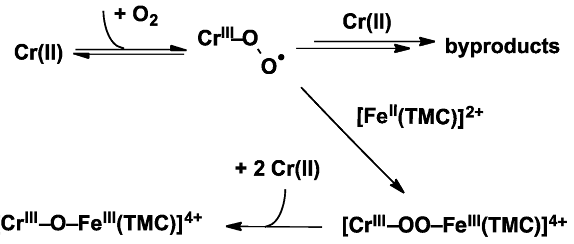

Scheme 1 Proposed mechanism for formation of **1** by O_2 activation.

inner-sphere electron transfer. The structure of **1** was deduced by a combination of UV-vis, resonance Raman, and X-ray absorption spectroscopic methods and ESI-MS. The O_2 activation mechanism for the formation of **1** is proposed to be analogous to that of cytochrome oxidase, where the initially formed O_2 adduct is reduced by the other three redox-active metal centers in the enzyme, demonstrating a general strategy for O_2 activation. Furthermore, **1** represents only the second example of a hetero-bimetallic M–O–Fe(TMC) complex, which can shed light on the effects of Lewis acidic metal centers on the redox properties of high-valent M = O species.[23] Such interactions are considered important for facilitating the oxidation of water by the $CaMn_4O_5$ cluster of the oxygen evolving complex in photosynthesis.[24–26] Along these lines, Lloret-Fillol and coworkers have demonstrated the formation of a related Fe^{IV}–O–Ce^{IV} intermediate in the oxidation of water by a nonheme iron catalyst with $Ce(NH_4)_3(NO_3)_6$ as oxidant.[27]

This work was supported by a grant from the US National Institutes of Health (GM-38767 to L.Q.) and a postdoctoral fellowship (GM-093479 to K.M.V.H.). XAS data were collected on Beamline X3B at the National Synchrotron Light Source, which is supported by the U.S. Department of Energy under Contract No. DE-AC02-98CH10886. Use of beamline X3B is made possible by the Center for Synchrotron Biosciences grant, P30-EB-00998, from the National Institute of Biomedical Imaging and Bioengineering. XAS data were also collected on Beamline 7-3 at the Stanford Synchrotron Radiation Lightsource, which is supported by the U.S. Department of Energy under Contract No. DE-AC02-76SF00515. Use of beamline 7-3 is supported by the DOE Office of Biological and Environmental Research, and by the National Institutes of Health, National Institute of General Medical Sciences (including P41GM103393).

References

1 I. Bertini, H. Gray, E. I. Stiefel and J. S. Valentine, *Biological Inorganic Chemistry: Structure and Reactivity*, University Science Books, 2007, pp. 319–442.

2 L. Que Jr. and W. B. Tolman, *Nature*, 2008, **455**, 333–340.

3 E. I. Solomon, D. E. Heppner, E. M. Johnston, J. W. Ginsbach, J. Cirera, M. Qayyum, M. T. Kieber-Emmons, C. H. Kjaergaard, R. G. Hadt and L. Tian, *Chem. Rev.*, 2014, **114**, 3659–3853.

4 S. Ferguson-Miller and G. T. Babcock, *Chem. Rev.*, 1996, **96**, 2889–2908.

5 T. Tsukihara, H. Aoyama, E. Yamashita, T. Tomizaki, H. Yamaguchi, K. Shinzawa-Itoh, R. Nakashima, R. Yaono and S. Yoshikawa, *Science*, 1996, **272**, 1136–1144.

6 W. Jiang, D. Yun, L. Saleh, E. W. Barr, G. Xing, L. M. Hoffart, M.-A. Maslak, C. Krebs and J. M. Bollinger, *Science*, 2007, **316**, 1188–1191.

7 W. Jiang, D. Yun, L. Saleh, J. M. Bollinger Jr. and C. Krebs, *Biochemistry*, 2008, **47**, 13736–13744.

8 T. Chishiro, Y. Shimazaki, F. Tani, Y. Tachi, Y. Naruta, S. Karasawa, S. Hayami and Y. Maeda, *Angew. Chem., Int. Ed.*, 2003, **42**, 2788–2791.

9 E. Kim, E. E. Chufán, K. Kamaraj and K. D. Karlin, *Chem. Rev.*, 2004, **104**, 1077–1134.

10 E. E. Chufán, S. C. Puiu and K. D. Karlin, *Acc. Chem. Res.*, 2007, **40**, 563–572.

11 R. Hotzelmann, K. Wieghardt, U. Floerke, H. J. Haupt, D. C. Weatherburn, J. Bonvoisin, G. Blondin and J. J. Girerd, *J. Am. Chem. Soc.*, 1992, **114**, 1681–1696.

12 (*a*) S. Fukuzumi, Y. Morimoto, H. Kotani, P. Naumov, Y.-M. Lee and W. Nam, *Nat. Chem.*, 2010, **2**, 756–759; (*b*) M. Swart, *Chem. Commun.*, 2013, **49**, 6650–6652; (*c*) J. Prakash, G. T. Rohde, K. K. Meier, A. J. Jasniewski, K. M. Van Heuvelen, E. Münck and L. Que Jr., *J. Am. Chem. Soc.*, 2015, **137**, 3478–3481.

13 J.-U. Rohde, J.-H. In, M. H. Lim, W. W. Brennessel, M. R. Bukowski, A. Stubna, E. Münck, W. Nam and L. Que, Jr., *Science*, 2003, **299**, 1037–1039.

14 (*a*) F. Li, *PhD thesis*, University of Minnesota, 2011; (*b*) K. D. Koehntop, J.-U. Rohde, M. Costas and L. Que Jr., *Dalton Trans.*, 2004, 3191–3198; (*c*) X. Shan, J.-U. Rohde, K. D. Koehntop, Y. Zhou, M. R. Bukowski, M. Costas, K. Fujisawa and L. Que, Jr., *Inorg. Chem.*, 2007, **46**, 8410–8417.

15 D. M. Kurtz Jr., *Chem. Rev.*, 1990, **90**, 585–606.

16 S. C. Lee and R. Holm, *J. Am. Chem. Soc.*, 1993, **115**, 11789–11798.

17 J. F. Berry, E. Bill, R. García-Serres, F. Neese, T. Weyhermüller and K. Wieghardt, *Inorg. Chem.*, 2006, **45**, 2027–2037.

18 D. J. Liston, B. J. Kennedy, K. S. Murray and B. O. West, *Inorg. Chem.*, 1985, **24**, 1561–1567.

19 T. E. Westre, P. Kennepohl, J. G. DeWitt, B. Hedman, K. O. Hodgson and E. I. Solomon, *J. Am. Chem. Soc.*, 1997, **119**, 6297–6314.

20 A. Roe, D. Schneider, R. Mayer, J. Pyrz, J. Widom and L. Que Jr., *J. Am. Chem. Soc.*, 1984, **106**, 1676–1681.

21 (*a*) J. Sanders-Loehr, W. D. Wheeler, A. K. Shiemke, B. A. Averill and T. M. Loehr, *J. Am. Chem. Soc.*, 1989, **111**, 8084–8093; (*b*) H. Zheng, Y. Zang, Y. Dong, V. G. Young, Jr. and L. Que, Jr., *J. Am. Chem. Soc.*, 1999, **121**, 2226–2235.

22 J. Cho, J. Woo and W. Nam, *J. Am. Chem. Soc.*, 2010, **132**, 5958–5959.

23 (*a*) S. Fukuzumi, *Coord. Chem. Rev.*, 2013, **257**, 1564–1575; (*b*) W. Nam, Y.-M. Lee and S. Fukuzumi, *Acc. Chem. Res.*, 2014, **47**, 1146–1154.

24 J. Yano and V. Yachandra, *Chem. Rev.*, 2014, **114**, 4175–4205.

25 P. E. Siegbahn, *Acc. Chem. Res.*, 2009, **42**, 1871–1880.

26 E. Y. Tsui, J. S. Kanady and T. Agapie, *Inorg. Chem.*, 2013, **52**, 13833–13848.

27 Z. Codolà, L. Gómez, S. T. Kleespies, L. Que Jr., M. Costas and J. Lloret-Fillol, *Nat. Commun.*, 2015, **6**, 5865, DOI: 10.1038/comms6865.